Chapter 6
Enhancement in greenish-white photoluminescence of $Zn_3(VO_4)_2$ phosphor by Bi^{3+} doping

In this chapter, we have explored the photoluminescence properties of rare-earth free $Zn_{(3-x)}Bi_x(VO_4)_2$ (x=0, 0.01, 0.03, 0.05) phosphors. The XRD analysis validates the crystallite growth and reduction of microstrain after Bi^{3+} doping. The absorption study ascertains the shift in the absorption edge with Bi^{3+} doping. The prepared phosphors have near-UV excitation of 350 nm, which reduces visible light reabsorption. The host has broadband emission centered on 540 nm and is enhanced by the factor of 11 after 1% doping of Bi^{3+} ions. The emission enhancement is attributed to the improved crystallinity and reduced microstrain. The, Bi^{3+} doped $Zn_3(VO_4)_2$ phosphor can be used as a greenish-white emission source for optical devices.

6.1 Introduction

Inorganic phosphor has been extensively explored in various optoelectronic applications such as in white light-emitting diodes (wLEDs), spectral converters for solar cells, display devices, etc [53,141,168,190]. Primarily, the phosphors used in these applications are rare-earth-based and they suffer various disadvantages. As in the case of commercially available rare-earth-based wLEDs, the poor color-rendering properties and high correlated color temperature (CCT) are the major drawbacks [12,191]. In wake of this, many rare-earth-doped oxy-nitride, oxide or sulfide hosts for wLEDs have been reported. Among many rare-earth ions, Eu^{2+} and Ce^{3+} have been highly used with host [54,57,58,94,95,192]. Even so, Ce^{3+} and Eu^{2+} endure unpreventable reabsorption of the blue-green wavelength of photons. In addition to these drawbacks, all rare-earth ions require high purification and refinement techniques, which make them expensive. Moreover, these phosphors are synthesized in a reduced atmosphere, and require high sintering temperature, curbing their large-scale production [193–197]. Therefore, the need for rare-earth-free phosphors having near UV excitation, greater absorption in the visible range, and a low-cost synthesis process is desirable.

Among many phosphors, metal vanadate compounds have emerged as rare-earth-free luminescence materials and are thus investigated for their use in optoelectronic devices [25,173]. The self-activated vanadate phosphors show an intense charge transfer band in the near UV region owing to charge transfer from O^{2-} to V^{5+} in $[VO_4]$ tetrahedron [198]. The synthesis of vanadate phosphors requires low sintering temperature and they can emit efficiently in a visible region without the use of rare-earth ions, which makes them cost-effective, energy-efficient, and suitable to obtain high color rendering index (CRI). Recently, many compounds of the $M_3V_2O_8$ (M = Zn, Ca, Ba, Mg, and Sr) material system have been studied for photo-catalytic, and phosphor materials [18,25,199–201]. Our choice of

$Zn_3(VO_4)_2$ as a host is based on earlier reports which establish that $Zn_3(VO_4)_2$ has the strongest emission and highest value of quantum yield among other members of the $M_3V_2O_8$ material system [202,203]. The luminescence of the host material can be further improved by choosing a suitable activator ion. It is well known that trivalent bismuth ion has $^1S_0$ as its ground state and $^3P_1$ and $^1P_1$ as allowed excited states. The electronic transition between these levels is the source of photoluminescence properties of Bi^{3+} ions. The Bi^{3+} doped phosphors have been studied by the research fraternity owing to their broad emission in the visible region and its broad excitation band in the UV region which can avoid the reabsorption of visible photons [204,205]. The earlier report of Bi^{3+} doped $Zn_3(VO_4)_2$ lacks a correlation between the structural and optical properties. Moreover, a comparison between the PL emission of the host ($Zn_3(VO_4)_2$) and doped phosphors is also not established in previous reports. Also, our synthesis process is advantageous over the previously reported solid-state synthesis process [206].

In the present chapter, we report the optical properties of $Zn_3(VO_4)_2$ and $Zn_{(3-x)}Bi_x(VO_4)_2$ (x=0, 0.01, 0.03, 0.05) phosphors synthesized via the solution combustion process and correlate it with structural changes. The prepared phosphors have near UV excitation which eliminates chances of visible light reabsorption. Significant enhancement in the broadband PL emission by Bi^{3+} doping in the host is also observed. The overall emission of the phosphors gives greenish-white emission.

6.2 Materials and synthesis technique

6.2.1 Materials for the synthesis

Zinc nitrate hexahydrate ($Zn(NO_3)_2.6H_2O$, 99%, SRL chemicals), ammonium metavanadate (NH_4VO_3, 99%, Sigma-Aldrich), bismuth nitrate ($Bi(NO_3)_3$, 98%, Sigma-

Aldrich), urea (NH_2CONH_2), and double distilled water were used as materials for synthesis, without any further purification.

6.2.2 Preparation of Bi^{3+} doped $Zn_3(VO_4)_2$ phosphors.

The Bi^{3+} doped $Zn_3(VO_4)_2$ phosphors were prepared through the solution combustion process. We have synthesized $Zn_{(3-x)}Bi_x(VO_4)_2$ (x= 0, 0.01, 0.03, 0.05) phosphors having code names ZVO, ZVB1, ZVB3, and ZVB5, respectively. Sample preparation is discussed in Chapter 2.

6.2.3 Characterizations

The crystallinity and crystal structure of the prepared phosphors were validated by X-ray diffraction (XRD) using the Rigaku-MiniFlex-II DESKTOP powder X-ray diffractometer equipped with Cu K_α radiation (λ=1.54Å). The crystal structure was determined from the results of Rietveld refinement, which was performed using FULLPROF software [207]. The morphology of the phosphors was analyzed using a high-resolution scanning electron microscope (Nova Nano SEM 450, FEI) and the elemental validation was carried out by examining energy dispersive x-ray (EDX) spectra. The Fourier transform infrared (FTIR) scans were obtained in a range of 380 to 4000 cm^{-1} from the JASCO FT/IR 4600. Ultraviolet (UV) to Visible (Vis) absorption scans were recorded between 200 nm and 800 nm from the JASCO V770 UV-Vis-NIR spectrophotometer equipped with a barium sulfate-coated integrating sphere. Photoluminescence excitation (PLE) and emission (PL) scans were obtained from the Horiba Fluorolog-3 spectrophotometer equipped with a 450 W xenon flash lamp.

6.3 Results and discussion

6.3.1 Structural analysis

The validation of phase purity for ZVO and ZVB1 phosphors are made from the refinement of their respective XRD patterns, depicted in Fig. 6.1.

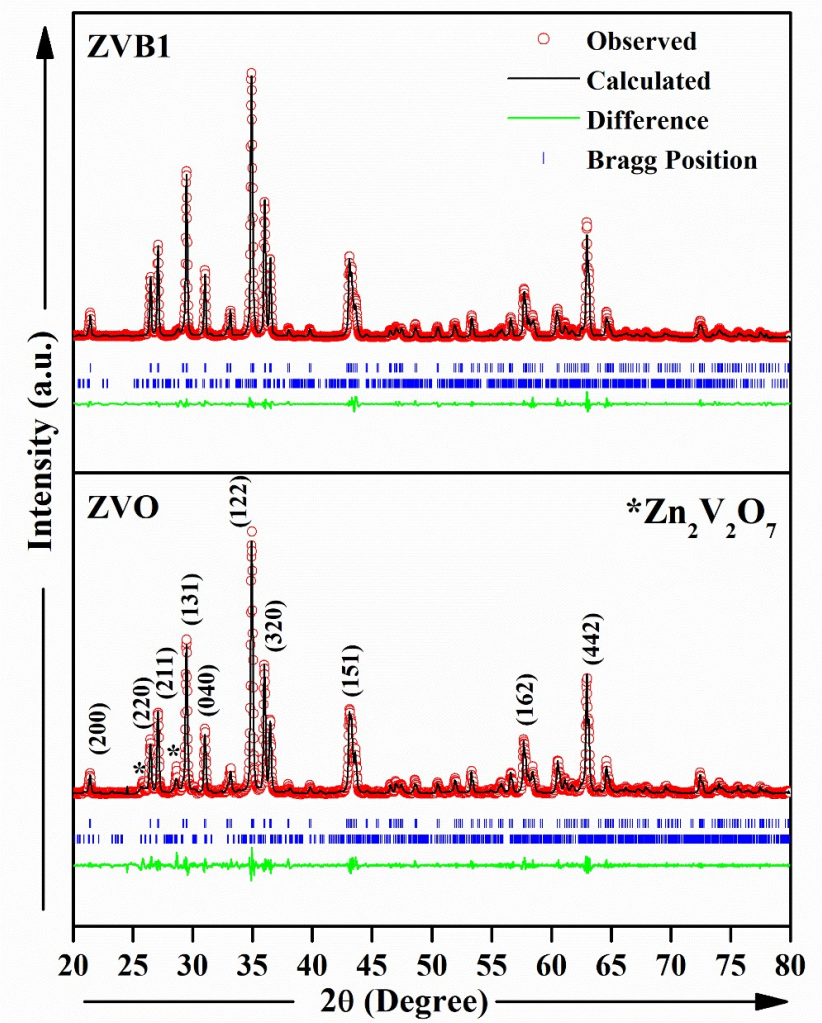

Fig. 6.1 Rietveld refinement of the room temperature XRD patterns of ZVO and ZVB1 phosphors. The '*' denotes $Zn_2V_2O_7$ having a C2/m (12) space-group.

The diffraction peaks match well with the standard $Zn_3(VO_4)_2$ orthorhombic phase (JCPDS card no. 34-0378). Some impurity peaks are observed which correspond to $Zn_2V_2O_7$ having a monoclinic phase (JCPDS card no. 016-0830) and are marked with '*' in Fig. 6.1. The prominent peaks for ZVO such as (200), (220), (211), (131), (040), (122), (320), (151),

(162), and (442) confirms that phosphors are crystallized as orthorhombic crystal structure with a space-group of Cmca. The Bi^{3+} doping has not resulted in any extra impurity peak. The lattice parameters and volume of the unit cell are obtained after the refinement and are listed in Table 6.1. The incorporation of Bi^{3+} ions in the lattice results in volume expansion. The refinement reveals that for ZVO, V ions occupy tetrahedral sites, while Zn ions occupy two types of octahedral sites. The Zn ions lying in a site with symmetry 2/*m* and having two different bond lengths are termed as Zn1, while Zn ions lying in a site with symmetry *m* and having three different bond lengths are termed as Zn2 [29]. The crystal structure is depicted in Fig. 6.2.

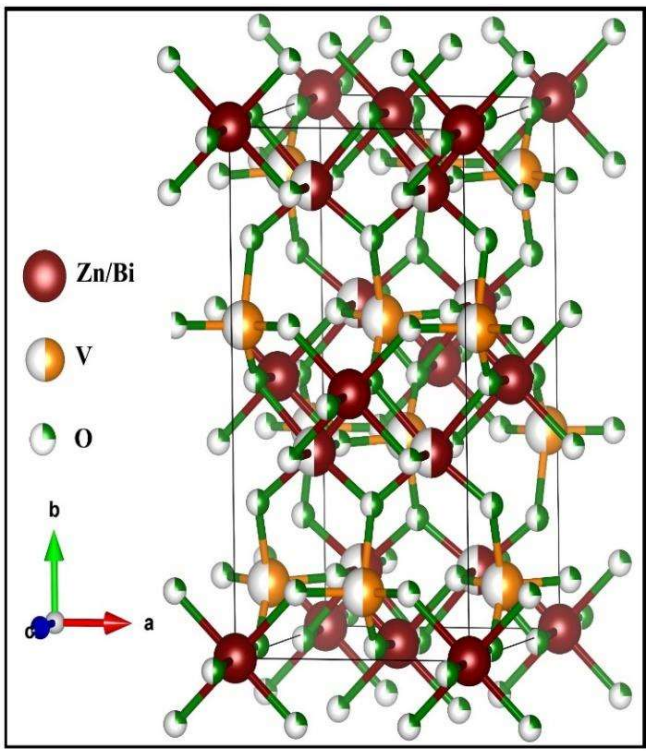

Fig. 6.2 Crystal structure of ZVO, drawn based on Rietveld refinement.

Table 6.1 Structural parameters after Rietveld refinement of ZVO and ZVB1 for the orthorhombic phase.

Parameters	ZVO	ZVB1
Atomic positions		
Zn1/Bi1 (x,y,z)	(0, 0, 0)	(0, 0, 0)
Zn2/Bi2 (x,y,z)	(0.25, 0.124, 0.25)	(0.25, 0.124, 0.25)
V (x,y,z)	(0, 0.380, 0.124)	(0, 0.381, 0.123)
O1 (x,y,z)	(0, 0.222, 0.234)	(0, 0.222, 0.224)
O2 (x,y,z)	(0, 0.990, 0.246)	(0, 0.991, 0.243)
O3 (x,y,z)	(0.242, 0.375, 0.006)	(0.241, 0.378, 0.003)
Angles (α, β, γ) in degree	(90, 90, 90)	(90, 90, 90)
Lattice parameters (Å)		
a	6.11	6.12
b	11.53	11.53
c	8.30	8.30
Volume ($Å^3$)	584.72	585.68
$R_{Factors}$		
R_p	10.9	7.76
R_{wp}	18.1	10.3
R_{exp}	12.18	3.49
χ^2	2.22	8.75

The variation in average crystallite size (*D*) with Bi^{3+} doping in $Zn_3(VO_4)_2$ is studied by the Scherrer equation. The well-known Scherrer formula which is used to estimate average crystallite size (*D*) is as follows;

$$D_{hkl} = \frac{K*\lambda}{\beta_D*\cos\theta} \quad (6.1)$$

Where D_{hkl} represents the crystallite size in the direction perpendicular to the lattice plane having h, k, and l as its miller indices, K is the crystallite shape factor approximately taken as 0.9, β_D is the resultant full width at half maximum (FWHM) of the XRD peak after deducting instrumental broadening, and the wavelength of the x-ray radiation and the Bragg

angle is denoted by λ and θ, respectively [208]. The obtained values for crystallite size are 46 nm and 52 nm for ZVO and ZVB1, respectively. It is thus observed that Bi^{3+} ions assist the growth of crystallites.

The Scherrer equation does not take into account the effect of microstrain on the peak broadening. Williamson-Hall equation considers peak broadening due to crystallite size as well as due to microstrain. The broadening due to microstrain is given by equation 6.2

$$\beta_\epsilon = 4\epsilon\tan\theta \tag{6.2}$$

The resultant peak broadening is then the sum crystallite size broadening (β_D) and microstrain broadening (β_ϵ).

$$\beta_{hkl} = \beta_D + \beta_\epsilon \tag{6.3}$$

Using the value of β_D from the Scherrer equation and after rearranging, the resultant Williamson-Hall equation for estimating the crystallite size (D) and microstrain (ϵ) is [209],

$$\beta_{hkl}\cos\theta = 4\epsilon\sin\theta + \frac{K\lambda}{D}, \tag{6.4}$$

The W-H plot between $\sin\theta$ and $\beta_{hkl}\cos\theta$ for ZVO and ZVB1 is linearly fitted. The slope of the linearly fitted line gives crystallite size (D). The crystallite size for ZVO and ZVB1 is 68 nm and 75 nm, respectively. The increase in crystallite size again confirms that Bi^{3+} ions assist the growth of crystallites. The improvement in the crystallinity of the sample and the growth of crystallites of the sample via doping Bi^{3+} ions for the different hosts is also reported earlier [209]. The microstrain which is a measure of crystal lattice relaxation is also obtained from the W-H plot. The intercept of the fitted line is used to determine the microstrain (ϵ). It is observed that the microstrain for ZVO and ZVB1 is 10.2×10^{-4} and 8.6

$\times 10^{-4}$, respectively. Thus, we can infer that because of Bi^{3+} ion doping in the $Zn_3(VO_4)_2$ crystal lattice, the microstrain is reduced. The reduced strain indicates towards ordering of crystal structure. The decrease in microstrain decreases the crystal defects present in the phosphor which suggest improvement in the local crystal structure of the phosphor with Bi^{3+} co-doping. The ordering of crystal structure help in improving emission [209].

6.3.2 Morphological and elemental analysis

The HR-SEM analysis is used to examine the effect of Bi^{3+} doping on the morphology of $Zn_3(VO_4)_2$. The HR-SEM micrographs of all the prepared phosphors are presented in Fig. 6.3. The ZVO sample shows signs of agglomeration which is reduced by doping Bi^{3+} ion. The surface of grains for Bi^{3+} doped samples appears to be smoother than the host sample. The calculated average grain diameter for ZVO, ZVB1, ZVB3, and ZVB5 are 156 nm, 170 nm, 189 nm, and 202 nm, respectively. It is observed that the calculated average grain size is increased by doping Bi^{3+} ions in the host matrix and thus supports the crystallite size calculation from XRD analysis.

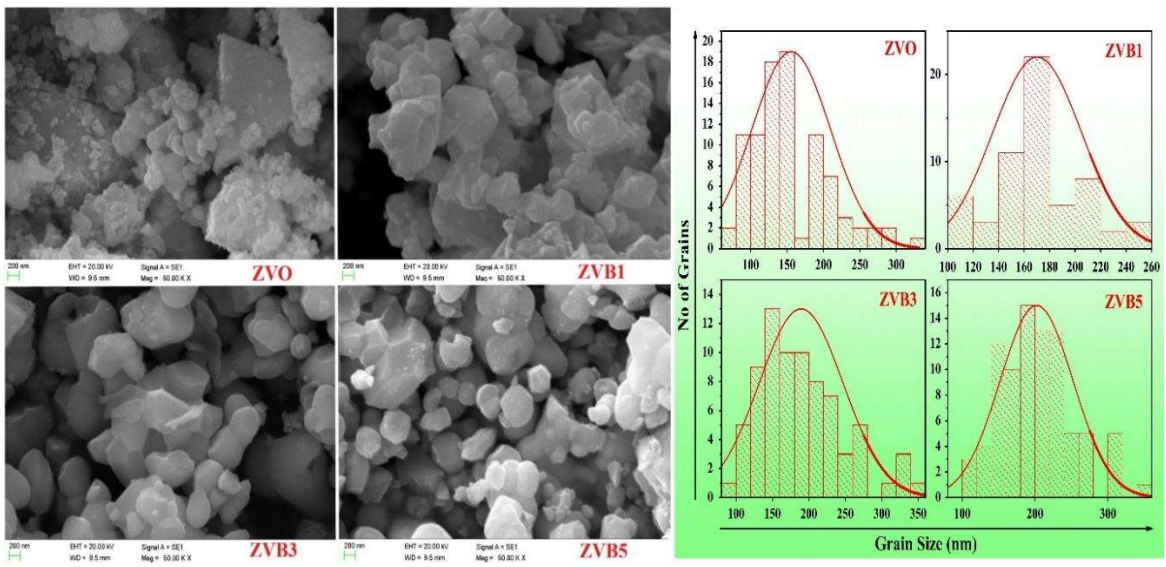

Fig. 6.3 SEM images for all samples.

The chemical composition profile for a particular sample can be estimated by the EDX spectra. The EDX spectra for ZVB1 shown in Fig. 6.4 confirm the presence of elements in the prepared phosphor.

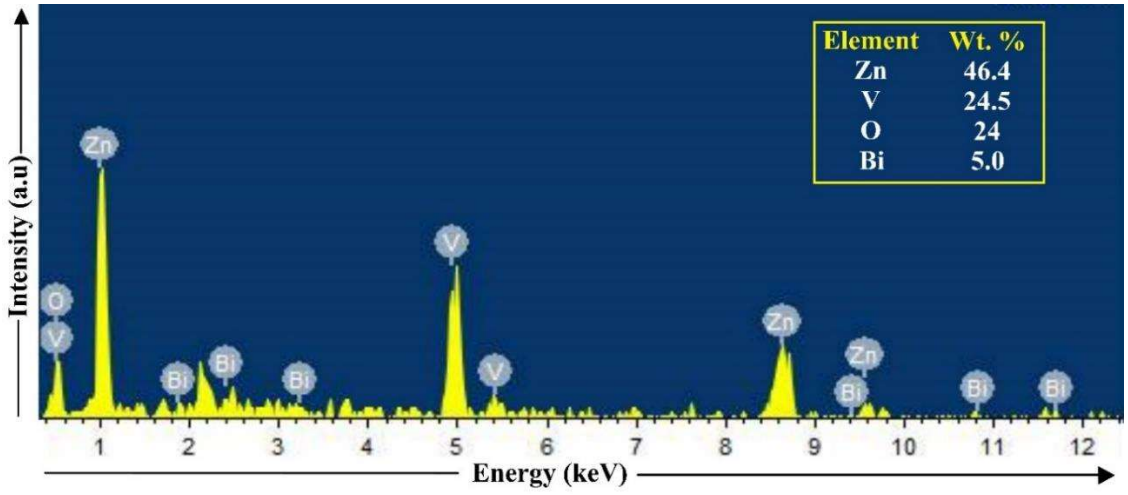

Fig. 6.4 EDS spectra of $Zn_3(VO_4)_2$:Bi(1%) phosphor.

6.3.3 Infrared spectroscopy analysis

The vibrational bands present in a particular sample can be analyzed by FTIR spectroscopy. The FTIR scans of all the phosphors were recorded over the range of 380 cm^{-1} to 4000 cm^{-1} and are presented in Fig. 6.5. The weak vibrational band from 400-425 cm^{-1} corresponds to Zn-O stretching vibrations [210]. The intense broad peak around 600-700 cm^{-1} corresponds to tetrahedral VO_4 vibrational modes [210]. The peak centered around 788 cm^{-1} is ascribed to asymmetric (V-O-Zn) and (V-O-V) vibrations [36]. The IR vibrational band from 814-845 cm^{-1} is ascribed to the stretching vibration of the V-O bond [211]. The intense band centered on 2363 cm^{-1} ascribed to CO_3^{2-} stretching vibration [212]. The vibrational modes corresponding to hydroxyl groups are not detected in FTIR analysis. The observed vibrational bands for all samples support XRD results by indicating that their crystalline phase has formed.

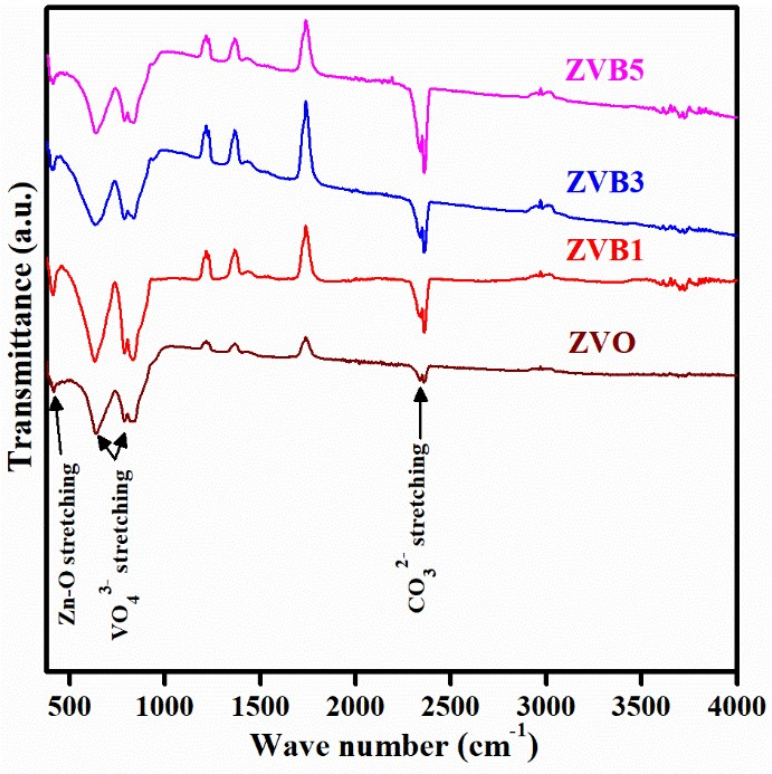

Fig. 6.5 FTIR spectrum of all phosphors.

6.3.4 Absorption study

Fig. 6.6 (a) depicts the UV-Vis absorption scans of all the prepared samples. The broad absorption peak of ZVO is centered at 326 nm and is ascribed to the ligand to metal charge transfer transition from O^{2-} to V^{5+} in $[VO_4]$ tetrahedral. The Bi^{3+} doped phosphors show a shift in absorption edge which is because of absorption to metal to metal charge transfer (MMCT) band of $Bi^{3+} - V^{5+}$ formed below $^1T_2$ and $^1T_1$ levels of $[VO_4]$ tetrahedral. The discussion on the formation of MMCT is done later in the photoluminescence section.

The Urbach energy can be used to estimate the extent of disorder in the host lattice introduced due to doping. The Urbach energy (E_u) and the absorption coefficient (α) is related by the equation 6.5 [213],

$$\alpha = \alpha_0 e^{\left(\frac{h\vartheta}{Eu}\right)} \tag{6.5}$$

Where $h\vartheta$ represents the photon energy and α_0 is a constant. The linear part of $\ln(\alpha)$ vs $h\vartheta$ plot is fitted and the reciprocal of its slope is used to deduce the Urbach energy. The $\ln(\alpha)$ vs $h\vartheta$ plot for ZVB1 is presented in Fig. 6.6 (b) and the variation of E_u with samples is shown in the inset. The calculated E_u for ZVO is 0.78 eV and decreases with doping Bi ions in the host, which is a good validation of an increase in the crystallinity of the prepared phosphors [213].

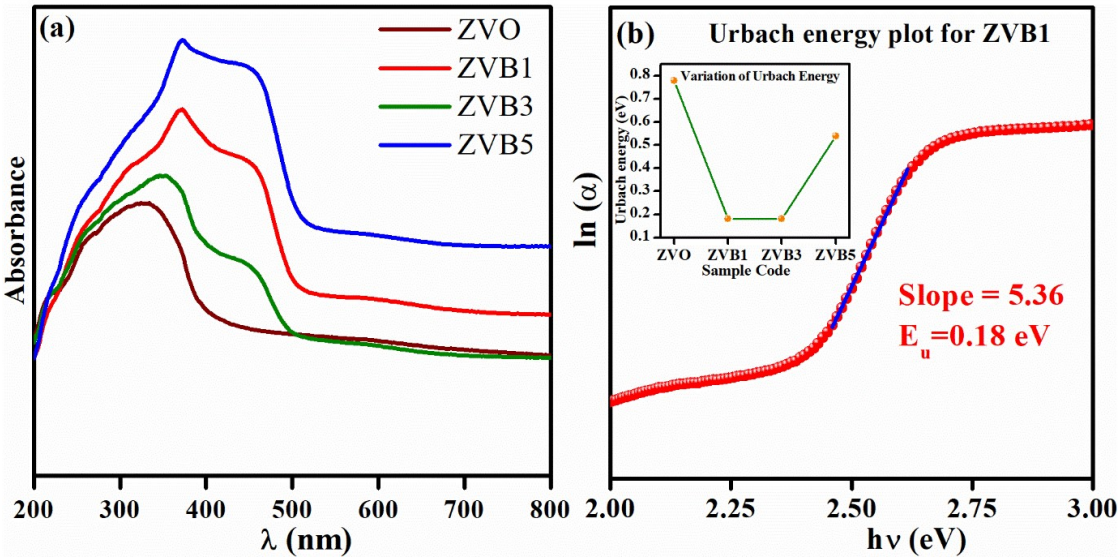

Fig. 6.6 (a) Absorbance spectrum of all prepared phosphors. **(b)** Urbach energy plot for ZVB1, where the blue line shows a linearly fitted portion of the graph. The inset in figure b shows the variation of Urbach energy with prepared phosphors.

6.3.5 Photoluminescence study

Fig. 6.7 depicts the PLE spectra for all the prepared phosphors monitored at 542 nm emission wavelength. The near UV broadband for $Zn_3(VO_4)_2$ was observed around 340 nm and is accredited to $^1A_1 \rightarrow {}^1T_1$ and $^1A_1 \rightarrow {}^1T_2$ electronic transitions in a VO_4 tetrahedron [203]. The $^1A_1$ ground state is made up of the O 2p orbitals while $^1T_1$ and $^1T_2$ excited states are composed of V 3d orbitals. The UV photons excite electrons from the $^1A_1$ ground state to the $^1T_1$ and $^1T_2$ excited states. The excitation process from $^1A_1$ to $^3T_1$ and $^3T_2$ is spin forbidden [203]. The PLE spectra for Bi^{3+} doped $Zn_3(VO_4)_2$ is also a broadband spectrum with

a peak at 352 nm. The increase in excitation peak for doped phosphors suggests that Bi^{3+} ions increase the energy absorption of the host. The excitation peak for the doped phosphors is red-shifted as compared to the host. The shift in the PLE spectrum can be understood by deconvoluting the PLE spectrum of ZVB1 as depicted in Fig. 6.7 (b). The deconvoluted peaks at lower energy correspond to the transition from the ground state to the metal-metal charge transfer (MMCT) band formed after Bi^{3+} doping and the peak at higher energy (~4 eV) corresponds to $^1A_1 \rightarrow {}^1T_1$ electronic transition of $[VO_4]^{3-}$ ion. The shift in the excitation edge towards the higher wavelength (or lower energy) is attributed to the formation of the MMCT band after Bi^{3+} doping [10]. The excited MMCT state is formed because of the transitions between $Bi^{3+}(6s^2) - V^{5+}(3d^0)$ and $Bi^{4+}(6s^1) - V^{4+}(3d^1)$ configurations [10]. The excitation band for Bi^{3+} doped $Zn_3(VO_4)_2$ matches well with the commercially available GaN or InGaN-based UV/nUV LED chips which make it useful for LED application.

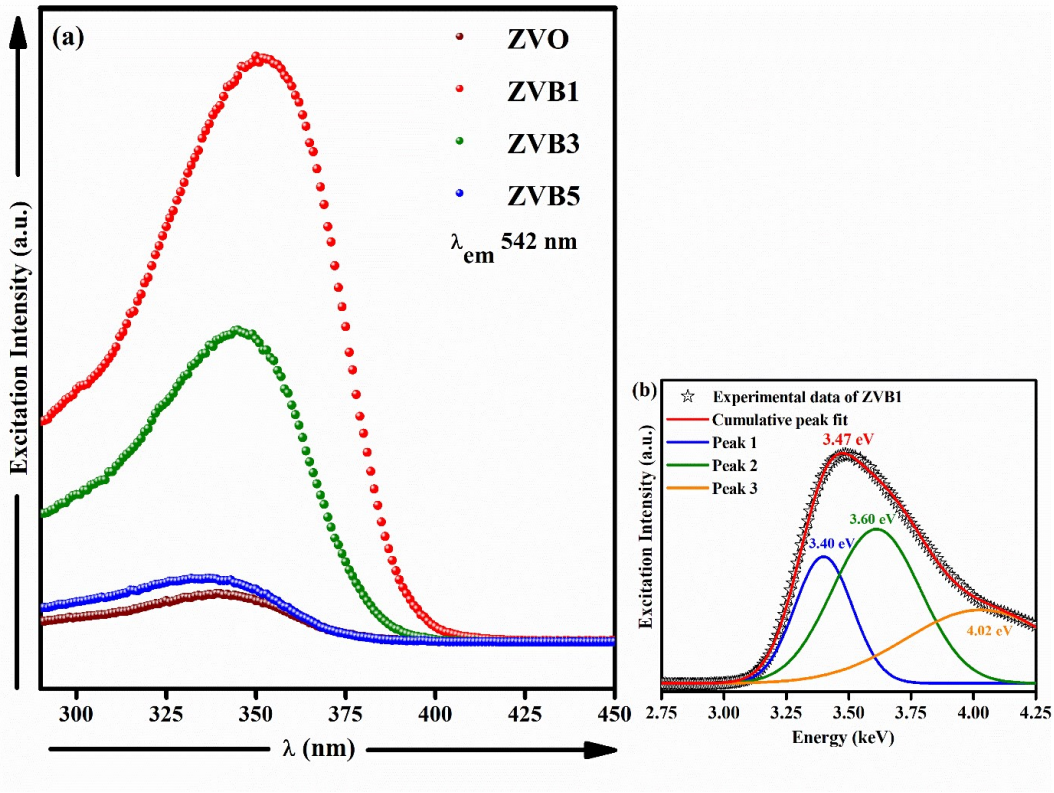

Fig. 6.7 (a) Photoluminescence excitation spectrum of prepared phosphors for 542 nm emission wavelength. **(b)** Peak fitting of ZVB1 excitation spectra.

Fig. 6.8 (a) depicts the PL spectra of all samples, examined at 340 nm excitation wavelength. The broadband emission spectrum of the ZVO is ascribed to the transitions from $^3T_2$ and $^3T_1$ excited states to the $^1A_1$ ground state of V^{5+} ion in tetrahedral $[VO_4]^{3-}$ group [203]. The Bi^{3+} doped $Zn_3(VO_4)_2$ shows a significant increase in the emission intensity. The emission intensity of ZVB3 and ZVB5 is less than that of ZVB1 because on increasing the concentration of Bi^{3+} ions the non-radiative energy transfer between the Bi^{3+} ions increases.

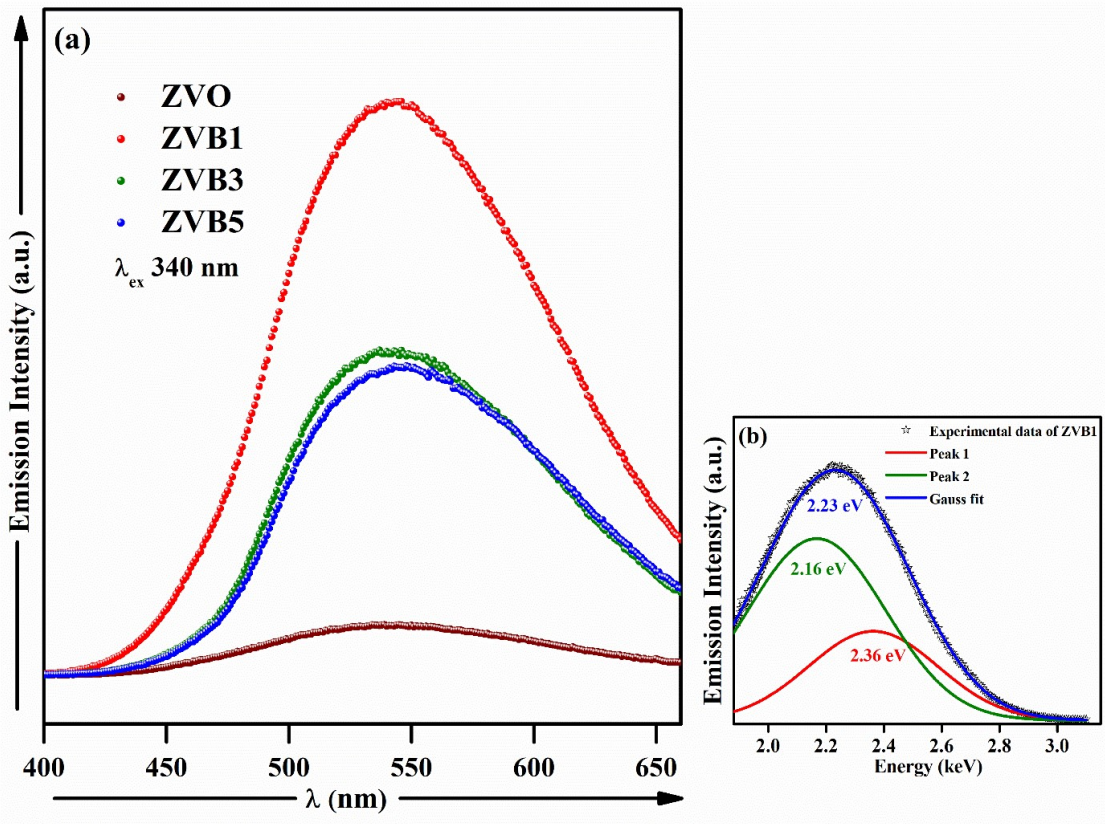

Fig. 6.8 (a) Photoluminescence emission spectrum of prepared phosphors for 340 nm excitation wavelength. **(b)** Peak fitting of ZVB1 emission spectra.

The non-radiative energy transfer among the luminescent centers can be realized by exchange interactions or multipolar interactions. In exchange interaction, the energy is transferred among the Bi^{3+} ions and then non-radiatively to the lattice defects in the form

of phonons. According to Blasse's theory, the critical distance (R) between the Bi^{3+} ions at which the energy transfer occur is given by the following formula [214],

$$R = 2\left(\frac{3V}{4\pi cN}\right)^{\frac{1}{3}} \quad (6.6)$$

Where the volume of the unit cell is represented by *V*, the concentration of Bi^{3+} for maximum emission intensity by *c*, and the number of Zn^{2+} sites that can be occupied by the Bi^{3+} ions in a unit cell by *N*. For this study, c is 0.01, N is 12 and V is 385.17 $Å^3$. The calculated value of R is 21.04 Å. According to Blasse et.al [214], the critical distance necessary for non-radiative energy transfer from acceptor to donor ions must be less than 5 Å. Therefore, in our case the exchange interactions are unlikely and quenching could be the result of electric multipolar interactions.

6.3.6 Effect of Bi^{3+} doping on the photoluminescence spectrum

The Bi^{3+} doping enhances the emission intensity of the ZVO phosphors. The XRD analysis manifests that the crystallite size of the phosphor is increased with increasing Bi^{3+} concentration. The crystallite size has improved from 68 to 75 nm for ZVO and ZVB1, respectively. As a result of improved crystallinity, the particle size also increases while the surface-to-volume ratio decreases [138,215]. The surface of particles has more defect centers, therefore, the number of ions interacting with defect centers decreases by decreasing the total surface area, and the number of emitting ions in crystallites increases. Thus, the quenching centers in the form of site defects are eliminated [138,139,208,209,215]. Secondly, because the microstrain is reduced by Bi^{3+} doping, the crystal defects present in the phosphor are reduced and the crystal structure becomes more ordered. The ordering of crystal structure helps in improving the emission intensity [209,216].

The schematic in Fig.9 (a) illustrates the energy transfer dynamics in $Zn_3(VO_4)_2:Bi^{3+}$ system. The excitation of $[VO_4]^{3-}$, around 310 nm (~4 eV), results from the $^1A_1 \rightarrow {}^1T_1$ electronic transition. The excitation process is followed by the intersystem crossing from $^1T_1$ to $^3T_{1,2}$ states and $^3T_{1,2} \rightarrow {}^1A_1$ electronic transition, which results in the emission from $[VO_4]^{3-}$ ion, around 526 nm (~2.36 eV). The Bi^{3+} doping forms the MMCT band in $Zn_3(VO_4)_2:Bi^{3+}$ system below $^3T_{1,2}$ levels, and the electronic transition from this band to $^1S_0$ level of Bi^{3+} results in emission around 574 nm (~2.16 eV). The increase in the emission intensity of the phosphor by Bi^{3+} doping is attributed to the improved crystallinity, increased particle size and reduced microstrain. The emission intensity is increased by the factor of 11 after 1% Bi^{3+} doping in the $Zn_3(VO_4)_2$ system.

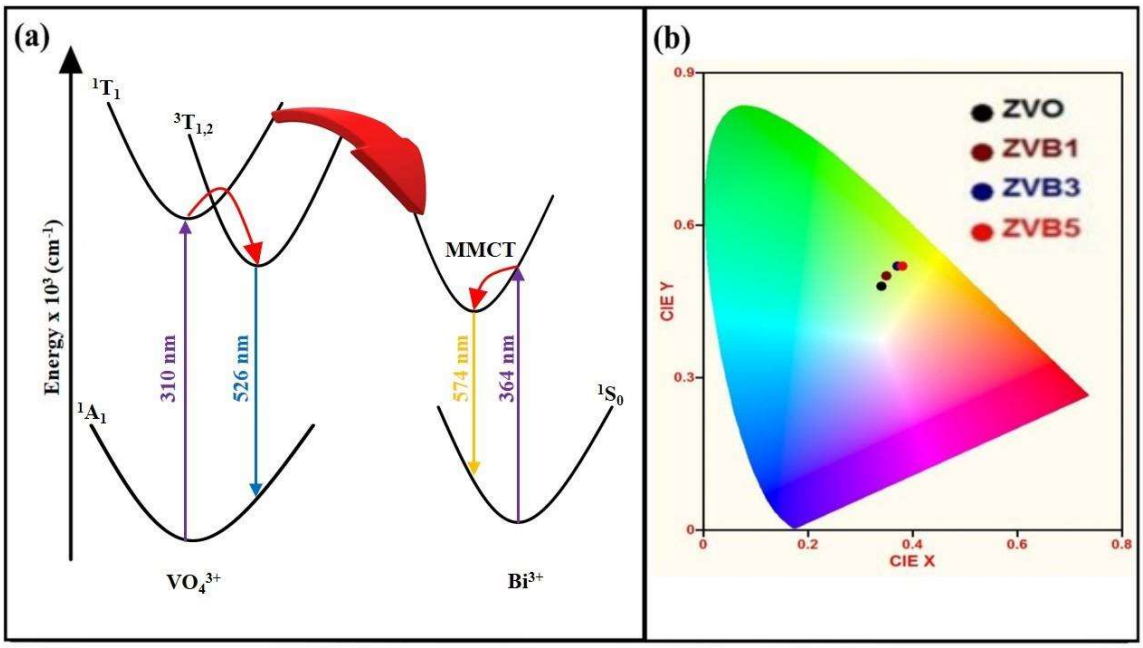

Fig. 6.9 (a) Schematic of energy transfer among $[VO_4]^{3-}$ energy levels and from $[VO_4]^{3-}$ to MMCT band. **(b)** CIE coordinates for all the prepared phosphors.

6.3.7 CIE coordinates

The Commission Intentional de I'eclairage (CIE) coordinates can be used to determine the luminescence colours of the samples. The calculated CIE coordinates (x,y) for ZVO,

ZVB1, ZVB3 and ZVB5 are (0.343, 0.477), (0.355, 0.502), (0.368, 0.521), and (0.376, 0.519), respectively and are depicted in Fig.9 (b). We can infer that ZVO and ZVB1 have greenish-white emission and on increasing the concentration of Bi^{3+} the overall emission shift towards greenish-yellow, which is reflected in their CIE coordinates. On account of maximum emission intensity, near UV excitation, and calculated CIE coordinates, ZVB1 is the most suitable for rare-earth free white LEDs.

6.4 Conclusions

In summary, we have the phase purity of the phosphors is validated by XRD and FTIR analysis. The XRD analysis ascertains the crystallite size growth and reduction in microstrain with Bi^{3+} ion doping. The analysis of Urbach energy validates improvement in crystallinity for Bi^{3+} doped phosphors. The PLE study reveals that $Zn_{(3-x)}Bi_x(VO_4)_2$ phosphors have near-UV excitation which avoids visible light reabsorption. Moreover, a significant increase and redshift in excitation peak after Bi^{3+} doping is observed. The PL emission intensity of ZVO is significantly enhanced by the factor of 11 after Bi^{3+} doping. The PL emission enhancement is accredited to an improvement in crystallinity, improved morphology, and ordering of local crystal structure by Bi^{3+} doping. Thus, from our study we propose $Zn_{(3-x)}Bi_x(VO_4)_2$ phosphors as rare-earth free and cost-efficient material for phosphor-optoelectronic devices.